Synthetic Glycosidase Distinguishing Glycan and Glycosidic Linkage in Its Catalytic Hydrolysis

Xiaowei Li and Yan Zhao*

Department of Chemistry, Iowa State University, Ames, Iowa 50011-3111, USA

ABSTRACT: Selective hydrolysis of carbohydrates is vital to the processing of these molecules in biology but has rarely been achieved with synthetic catalysts. The challenge is especially difficult because the catalyst needs to distinguish the inversion of a single hydroxyl and the α or β glycosidic bonds that join monosaccharide building blocks. Here we report synthetic glycosidase prepared through molecular imprinting within a cross-linked micelle. The nanoparticle catalyst resembles natural enzymes in dimension, water-solubility, and a hydrophilic/hydrophobic surface–core topology. Its boronic acid-functionalized active site binds its targeted glycoside substrate and an acid cofactor simultaneously, with the acidic group in close proximity to the exocyclic glycosidic oxygen. The hydrophobically anchored acid cofactor is tunable in acidity and causes selective cleavage of the targeted glycoside in mildly acidic water. Selectivity for both the glycan and the α/β glycosidic bond can be rationally designed through the molecular imprinting process.

KEYWORDS: *molecular imprinting, hydrolysis, artificial enzyme, selectivity, Michaelis-Menten, active site, biomimetic catalysis*

INTRODUCTION

Carbohydrates are the most abundant biomolecules on earth and serve a plethora of functions including energy storage, structural support, cell signaling, and immune response.[1-3] Unlike proteins and nucleic acids that are linear polymers created through a sequence template, glycans in a biological system can be linear or branched, with great structural diversity depending on multiple factors including the concentrations of the enzymes involved in the biosynthesis.[4] Not only different monomer building blocks can be used in the construction, the sugar residues can be connected at different sites, via either α or β glycosidic bonds.

Most organisms use 1–3% of their genome to encode proteins for the synthesis and hydrolysis of carbohydrates.[5] The majority of these enzymes, however, cannot be obtained easily and new chemical tools are in urgen need to manipulate carbohydrates, whether in analytical or functional glycomics.[4] In addition, enzymes tend to have narrow operating windows and robust catalysts with glycosidic activities are required for challenging operations such as biomass conversion.[6]

The glycosidic linkages between sugar residues in a glycan are acetal or ketal. Their hydrolysis in principle can be achieved simply using acidic water. The difficulty lies in the selectivity of the process: since the monomeric building blocks, connection sites, spatial orientation of the glycosidic linkage, and overall topology of the oligo- or polysaccharide all profoundly influence the chemical and biological properties of a glycan,[4] an effective synthetic glycosidase needs to differentiate these features.

Despite the importance of selective glycan hydrolysis to biology and chemistry, only a handful synthetic glycosidases have appeared in the literature, likely due to the general difficulty in molecular recognition of carbohydrates in water.[7] The earliest such example was reported by Bols and co-workers, who used an acid-functionalized cyclodextrin to hydrolyze *p*-nitrophenyl β-D-glucopyranoside, taking advantage of the macrocycle's ability to bind the algycon.[8,9] Other examples include the binuclear copper catalysts by Striegler that could hydrolyze aryl glycosides under basic conditions[10,11] and azobenzene-3,3′-dicarboxylic acid, which was shown by Bandyopadhyay et al. to hydrolyze *p*-nitrophenyl β-D-glucopyranoside in a photoresponsive manner.[12] Selectivity for different sugars and α/β anomers was even rarer among synthetic catalysts. Yu and Cowan conjugated a copper-binding motif to the sugar-binding domain of odorranalectin (a natural lectin-like peptide) and used the resulting synthetic metalloenzyme to remove fucose by oxidative cleavage.[13]

We recently reported molecularly imprinted nanoparticles (MINPs) as "synthetic lectins" that bound complex carbohydrates through reversible boronate bonds.[14,15] The binding selectivity was derived from the size/shape of the imprinted site, as well as the number and orientation of the sugar-binding groups installed through the molecular imprinting process. In this work, we describe a method to introduce an acid catalyst in the close proximity of the exocyclic glycosidic oxygen of a glycan, thus converting a MINP lectin into a synthetic glycosidase. The noncovalently anchored acid catalyst (i.e., cofactor) could be swapped via a "plug-and-play" fashion to modulate the catalytic activity. Most importantly, these catalysts displayed selectivity for both the glycan and the glycosidic linkage of the substrate—a previously unachieved goal with synthetic systems.

RESULTS AND DISCUSSION

Design and synthesis of MINP-based synthetic glycosidase. Wulff and co-workers pioneered in the synthesis of molecularly imprinted polymers (MIPs) for sugar recognition.[16-18] It is also known that both boronic acid[19-23] and boroxole[24-26] can be used to bind the diols on a sugar. However, to perform selective hydrolysis of a glycan, a catalyst must not only recognize the glycan but also have a catalytic group positioned close to the glycosidic bond for its selective catalysis. Even though MIPs have been used for catalysis,[27-35] insolubility and other challenges associated with traditional imprinted materials makes it challenging to create well-defined active sites with accurately positioned catalytic groups.

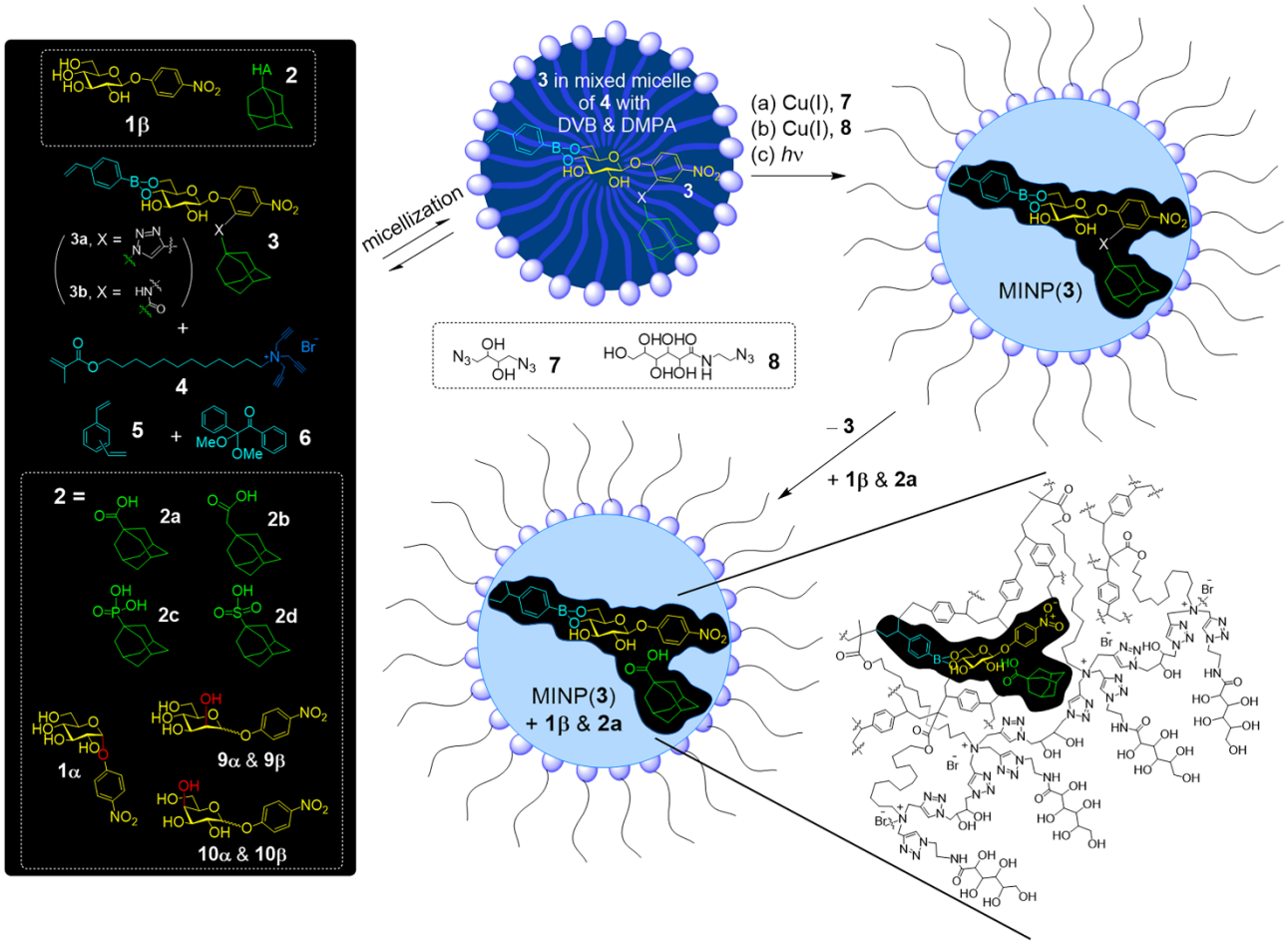

Scheme 1. Preparation of artificial glucosidase by micellar imprinting, with a schematic representation of the cross-linked structure.

Scheme 1 shows the preparation of water-soluble, protein-sized synthetic glycosidase for *p*-nitrophenyl β-D-glucopyranoside **1β** as a model substrate. This particular substrate is frequently used to evaluate the performance of both natural and synthetic glycosidase,[8-12] because its hydrolysis can be monitored conveniently by UV-vis spectroscopy.

The most challenging aspect of building an artificial enzyme is probably in the creation of a complex-shaped multifunctional active site.[36-38] Our strategy was to use boronate **3** as the template–functional monomer (FM) complex for molecular imprinting within a cross-linked micelle. Its color-coded structure contains a substrate-like (yellow) and a catalyst-like (green) moiety, with the latter placed near the exocyclic glycosidic oxygen by the *ortho* substitution of the phenyl ring. In addition, the 4,6-diol of the glucoside is known to form boronate ester bonds with the cyan-colored 4-vinylphenyl boronic acid.[16,21-23,39] A triazole linkage was used in **3a** and an amide in **3b**.

Micellar imprinting involved first solubilization of **3** in water by the micelle of **4**, together with divinyl benzene (DVB, **5**) as a core-cross-linker and 2,2-dimethoxy-2-phenylacetophenone (DMPA, **6**, a photoinitiator). The mixed micelle was cross-linked on the surface via diazide **7** by the highly efficient click reaction. A 1:1.2 ratio between **4** and **7** in the surface-cross-linking left the micelle with sufficient alkyne groups on the surface, allowing it to be decorated with a layer of hydrophilic ligand by monoazide **8** by another round of click reaction. The surface ligand not only increased the hydrophilicity of the cross-linked micelle but also endowed it with solubility for easy purification (i.e., precipitation from acetone and washing with organic solvents). Free-radical polymerization/cross-linking under UV-irradiation was key to the imprinting, not only solidifying the micellar core but also covalently attaching the boronic acid FM to the micelle via its polymerizable styrenyl group. The surface- and core-cross-linking could be monitored by ^{1}H NMR spectroscopy (Figures S1–3). The size of the MINP catalyst was measured to be ~5 nm by dynamic light scattering, which translates to ~50,000 Dalton in molecular weight (Figure S4–6). The size was also confirmed by transmission electron microscopy (Figure S7).

Template–FM complex **3** was designed to yield three features in the final MINP: a substrate-shaped binding site, a diol-binding boronic acid group, and an adamantane-shaped hydrophobic pocket near the glucose-binding site. The benefit of using covalent imprinting is the high-fidelity of the imprinting process, since polymerization and cross-linking turn the template–FM complex into part of the polymer network.[18,27,28] The difficulty, often times, is in the removal of the template from the highly cross-linked polymer.

In our case, the amphiphilicity of **3** helped it stay near the micelle surface, making the imprinted site highly accessible and the template easy to remove.[40] For these reasons, the templating glycoside could

Table 1. ITC binding data for *p*-nitrophenyl glycopyranosides and acid catalysts by MINP(**3a**) and MINP(**3b**).[a]

entry	MINP	pH	guest	K_a ($\times 10^4$ M^{-1})	ΔG (kcal/mol)	ΔH (kcal/mol)	$T\Delta S$ kcal/mol)	N [b]
1	MINP(**3a**)	6.0	**1β**	8.59 ± 0.67	-6.73	-8.84 ± 0.29	-2.11	1.14 ± 0.02
2	MINP(**3a**)	5.5	**1β**	1.49 ± 0.16	-5.69	-1.50 ± 0.08	4.19	1.27 ± 0.05
3	MINP(**3a**)	7.4	**1β**	14.0 ± 0.3	-7.02	-7.04 ± 0.05	-0.02	1.14 ± 0.01
4	NINP[c]	6.0	**1β**	<0.005	--	--	--	--
5	MINP(**3a**)	6.0	**1α**	2.49 ± 0.22	-5.99	-4.88 ± 0.20	1.11	1.18 ± 0.03
6	MINP(**3a**)	6.0	**9β**	4.18 ± 0.21	-6.30	-1.35 ± 0.02	4.9	0.79 ± 0.14
7	MINP(**3a**)	6.0	**9α**	0.17 ± 0.02	-4.42	-3.10 ± 0.39	1.32	1.29 ± 0.12
8	MINP(**3a**)	6.0	**10β**	0.90 ± 0.04	-5.39	-0.75 ± 0.01	4.64	1.49 ± 0.01
9	MINP(**3a**)	6.0	**10α**	0.13 ± 0.04	-4.24	-5.51 ± 4.34	-1.27	0.94 ± 0.22
10	MINP(**3a**)	6.0	PNP	0.34 ± 0.04	-4.82	-3.11 ± 0.76	1.71	0.85 ± 0.18
11	MINP(**3a**)	6.0	glucose	0.07 ± 0.001	-3.78	-4.71 ± 0.30	-0.93	0.74 ± 0.04
12	MINP(**3a**)	6.0	**2a**	122.0 ± 9.0	-8.30	-15.48 ± 0.14	-7.18	0.99 ± 0.01
13	MINP(**3a**)	5.5	**2a**	144.0 ± 7.6	-8.40	-40.28 ± 0.46	-31.88	0.87 ± 0.01
14	MINP(**3a**)	7.4	**2a**	35.8 ± 2.2	-7.57	-14.06 ± 0.22	-6.49	1.11 ± 0.01
15	MINP(**3a**)	6.0	**2b**	74.7 ± 3.5	-8.01	-12.02 ± 0.10	-4.01	1.02 ± 0.01
16	MINP(**3a**)	6.0	**2c**	36.6 ± 1.4	-7.58	-19.29 ± 0.22	-11.71	0.94 ± 0.01
17	MINP(**3a**)	6.0	**2d**	21.4 ± 1.3	-7.27	-2.73 ± 0.03	4.54	0.98 ± 0.01
18	MINP(**3b**)	6.0	**1β**	8.24 ± 0.60	-6.71	-22.80 ± 0.68	-16.09	1.07 ± 0.02
19	MINP(**3b**)	6.0	**1α**	2.46 ± 0.29	-5.99	-2.25 ± 0.16	3.74	1.12 ± 0.05
20	MINP(**3b**)	6.0	**2a**	14.20 ± 0.44	-7.02	-99.23 ± 2.26	-92.21	0.92 ± 0.02

[a] The titrations for all the glycosides, PNP, and glucose were performed in 10 mM MES buffer at 298 K. The titrations for the acid cofactors (**2a**–**2d**), which were not soluble in water, were performed in 10 mM MES buffer (pH 6.0) with 2% (v/v) DMSO. The ITC titration curves are reported in the Supporting Information (Figures S8-S27). [b] N is the average number of binding site per nanoparticle measured by ITC curve fitting. [c] Nonimprinted nanoparticles (NINPs) were prepared without any template. Binding was extremely weak. Because the binding constant was estimated from ITC, -ΔG and N are not listed.

be removed easily by solvent washing during the workup and purification. Consistent with the vacated binding site, the resulting MINP(**3a**) and MINP(**3b**) showed selectivity binding for both the targeted glycoside (**1β**) and the acid cofactors (**2a**–**2d**) (Table 1). The binding constants were determined by isothermal titration calorimetry (ITC), one of the most reliable methods to study intermolecular interactions.[41]

Table 1 (entry 1) shows that MINP(**3a**) bound the targeted **1β** with $K_a = 8.59 \times 10^4$ M^{-1}in pH 6 MES buffer. The binding constant approached those for monosaccharides by natural lectins ($K_a = 10^3$–10^4 M^{-1}).[2,42] The number of binding site determined by ITC was ~1.1, also supporting the vacated binding site. In our preparation, the surfactant/template ratio was generally maintained at 50, which is roughly the number of surfactant in the cross-linked micelle.[40] Such stoichiometry is expected to yield an average of one imprinted site per nanoparticle.

The binding of MINP(**3a**) for **1β** was sensitive to pH. A decrease of pH from 6 to 5.5 weakened the binding by nearly 6-fold, to $K_a = 1.50 \times 10^4$ $M^{-1}$and an increase to 7.4 strengthened the binding by 1.6-fold, to $K_a = 14.0 \times 10^4$ M^{-1} (Table 1, entries 1–3). The pH effect was similar to those observed in small-molecule boronic acids. A change of pH from 8.5 to 6.5, for example, reduces the binding between phenylboronic acid and glucose by 13-fold.[43] Molecular imprinting was key to the binding, as the nonimprinted nanoparticles showed negligible binding (entry 4). The imprinting factor, defined as the imprint/nonimprint binding ratio, was >1700 for **1β**.

We also studied the binding of MINP(**3a**) for several other glycoside analogues, including *p*-nitrophenyl α-D-glucopyranoside (**1α**), and the two anomers of both *p*-nitrophenyl D-mannopyranoside (**9α** and **9β**) and D-galactopyranosides (**10α** and **10β**) (Table 1, entries 5–9). The change from β to α glycosidic linkage lowered the binding by 3.4 times. Among the β glycosides, the binding followed the order of glucoside > mannoside > galactoside. The order supports the formation of the boronate ester bonds in the binding. As shown by the structures in Scheme 1, mannoside **9β** shared the same 4,6-*trans*-diol as glucoside **1β** and thus should be able to engage in the same boronate ester formation. Although the C2 hydroxyl was axial in **9β**, this particular hydroxyl was not expected to contribute to the binding as strongly as the boronate-forming C4 hydroxyl. For the same reason, inverting the C2 hydroxyl (in **9β**) only decreased the binding by roughly 2 times and inverting the C4 hydroxyl (in **10β**) decreased the binding by nearly 10 times. Not surprisingly, when both the glycan and the α/β glycosidic linkage were different from the template, the binding became even weaker (for α-mannoside **9α** and α-galactoside **10α**).

It is interesting to note that *p*-nitrophenol (PNP) showed a binding affinity in between the mismatched α glycosides (**9α** and **10α**) and the mismatched β glycosides (**9 β** and **10 β**). Since PNP could only occupy the imprinted site created from the *p*-nitrophenyl group of **3a**, the data suggest that the sugar residue contributed negatively to the binding of the *p*-nitrophenyl group in **9α** and **10α** but positively to the binding in **9β** and **10 β**. One way to do so is for the glycan to reside outside the sugar-binding pocket of the MINP for the mismatched α glycosides but inside, albeit with some difficulty, for the mismatched β glycosides.

Among the α glycosides, **1α** showed the strongest binding toward MINP(**3a**). Although this was not surprising because **9α** and **10α** differed from the "perfect guest" **1β** in both the glycan and the aglycon, it was puzzling why **1β** was bound only 3.4 times more strongly than the mismatched **1α**. One possibility is that, with the correctly matched glycan, there is a strong driving force for **1α** to occupy the sugar-binding site. Since MINP(**3a**) had a very large hydrophobic binding pocket (from PNP + adamantyl of the template), the PNP group might be able to fit within the imprinted site when the adamantyl pocket was vacant (vide infra).

Glucose does not have a hydrophobic aglycon and thus had nothing to occupy the *p*-nitrophenyl group-imprinted hydrophobic pocket of MINP(**3a**). Its extremely weak binding to the MINP suggests keeping the hydrophobic pocket empty while the sugar-binding site occupied was unfavorable. The much larger K_a of **1β** than the combined value from glucose and PNP indicates that the two groups work synergistically in the binding.

Acid cofactor **2** was expected to enter the adamantane-shaped binding site through hydrophobic interactions. The noncovalent, hydrophobic anchoring of the acid group enabled us to vary its acidity, as well as its distance to the bound substrate through **2a**–**d**. 1-Adamantanecarboxylic acid **2a** gave a very strong binding, with K_a = 122 $\times 10^4$ M^{-1}in pH 6 MES buffer, with 2 vol % DMSO added to aid solubility (Table 1, entry 12). This value was about 14 times larger than the K_a of **1β**. The difference reflects the importance of hydrophobic interactions in MINP binding in water,[40] which are proportional to the hydrophobic surface area buried upon binding.[44-46] Apparently, a single adamantyl was able to offer much stronger binding than the covalent boronate and the noncovalent binding of *p*-nitrophenyl combined.

The binding of MINP(**3a**) for **2a** increased at lower pH (Table 1, entries 12–14). Because a charged group is not solvated well and is unstable in a hydrophobic microenvironment,[47,48] the acid cofactor prefers to enter the MINP in its protonated, neutral state. Carboxylic acid has a pK_a of 4–5. The higher the solution pH, the stronger is the preference for the acid to be deprotonated in the solution, and the larger is the penalty the acid has to pay to enter the binding site in the protonated form.

For the different acid cofactors, the binding followed the order of **2a** > **2b** > **2c** > **2d** (Table 1, entries 12, 15–17). All the acid cofactors have the same adamantyl hydrophobe and thus should have a similar hydrophobic driving force to enter the imprinted site. However, a stronger acid has to overcome a larger unfavorable acid–base equilibrium to enter the binding pocket in the neutral form, and the binding is expected to be weaker. The weaker binding of **2b** in comparison to **2a** was most likely caused by the misfit of **2b** in the imprinted site. It was quite impressive that the MINP was able to detect the addition of a single methylene in the guest.

The binding site could be tuned additionally through the white-colored tether X (Scheme 1). The amide linkage in **3b** closely resembles the carboxylic acid of **2a** in dimension, whereas the triazole of **3a** was somewhat larger. ITC showed that MINP(**3b**) was an inferior receptor than MINP(**3a**) for acid cofactor **2a**. Since MINP(**3b**) was also inferior in catalysis (*vide infra*), we only studied its binding briefly. As shown by Table 1 (entries 18–20), its binding for the substrate (**1β**) and the **1β**/**1α** binding selectivity were very similar to those by MINP(**3a**), suggesting that the poor performance of MINP(**3b**) in catalysis derived from the weak binding of the acid cofactor.

There could be two possible reasons for the stronger binding of **2a** by MINP(**3a**) over MINP(**3b**). First, the secondary amide of **3b**, being an excellent hydrogen-bond donor and acceptor, could move the templated pocket for the adamantyl group closer to the micellar surface, by its strong solvation with water.[49] The shallower the imprinted pocket for the adamantyl group, the less hydrophobic would it be and the weaker was the driving force for **2a** to enter the pocket. Second, the imprinted pocket in MINP(**3b**) might be simply too tight for the acid cofactor. Micellar imprinting has been shown to have an extraordinary ability to reproduce structural features of the template due to the large imprinting factors (up to 10000 in some cases).[50-52] A move of a single methyl by one carbon, for example, was easily detected by peptide-template MINPs in their binding of isomeric di- and tripeptides.[53] The high fidelity was found to come from confining the imprinting (i.e., the templated polymerization/cross-linking) in the nanosized surface-cross-linked micelle.[54] Even though it is difficult to quantify the dimension of the imprinted site, we did expect template **3a** to afford a slightly larger space for the carboxylic acid group of **2a** than **3b**, which could be beneficial to the binding.

Hydrolysis of *p*-nitrophenyl glucopyranoside 1β. Figure 1a shows the hydrolysis of **1β** in pH 6 buffer at 40 °C. Both MINP(**3a**) and MINP(**3b**) showed significant activity over the background, with MINP(**3a**) being more active. The difference was consistent with a binding-controlled catalysis. For example, MINP(**3a**) bound the acid cofactor **2a** more strongly than the less efficient MINP(**3b**), by nearly 9 times (Table 1, entries 12 and 20). These K_a values translate to 51% and 87% of occupancy of MINP(**3a**) and MINP(**3b**) by the acid cofactor, respectively, at [MINP] = 5 μM and [**2a**] = 10 μM used for the hydrolysis. An increase of the **2a**/MINP ratio did increase the hydrolytic rate but minimal improvement was obtained beyond the 2:1 ratio (Table 2, entries 1–3).

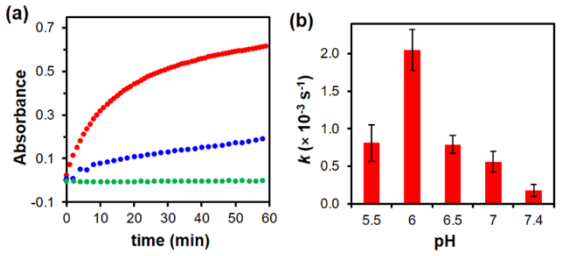

Figure 1. (a) Absorbance at 320 nm during the hydrolysis of **1β** in a 10 mM MES buffer (pH 6.0) (green filled circles), and in the presence of MINP(**3a**)+**2a** (red filled circles) or MINP(**3b**)+**2a** (blue filled circles) at 40 °C. (b) Effect of pH on the hydrolysis of **1β** catalyzed by MINP(**3a**)+**2a**. [**1β**] = 100 μM. [MINP] = 5 μM. [**2a**] = 10 μM.

Table 2. Pseudo-first-order rate constants for the hydrolysis of **1β** and by MINP(**3a**) under different conditions.[a]

entry	pH	acid cofactor	k ($\times 10^{-3}$ s^{-1})
1	6.0	5 μM **2a**	1.41
2	6.0	10 μM **2a**	2.05
3	6.0	15 μM **2a**	2.11
5	7.4	10 μM **2a**	0.18
6	7.0	10 μM **2a**	0.56
7	6.5	10 μM **2a**	0.79
8	5.5	10 μM **2a**	0.81
11	6.0	10 μM **2b**	1.36
9	6.0	10 μM **2c**	0.36
10	6.0	10 μM **2d**	0.14
11	6.0	15 μM **2a**	~0.002[b]

[a] Reaction were performed in 10 mM buffer at 40 °C with [MINP(**3a**)] = 5 μM. [b] Nonimprinted nanoparticles (NINPs) were used instead of MINP(**3a**).

A pH study showed that the hydrolysis showed a maximum at pH 6 for MINP(**3a**)+**2a** (Figure 1b). A screening of the different acid cofactors (**2a**–**2d**) indicated that an increase of acidity for the cofactor lowered the hydrolytic rates, in the order of **2a** > **2b** > **2c** > **2d** (Table 2). This trend was exactly the same as that found in the binding (Table 1), suggesting binding of the acid cofactor was the determining factor in the catalysis.

MINP(**3a**)+**2a** exhibited enzyme-like Michaelis–Menten kinetics in its hydrolysis of **1β** (Figure 2a). An excellent TON of 411 at 600 min when 500 equivalents of substrate were used in the hydrolysis (Figure 2b). The larger TON indicates the catalyst was very robust. Nonetheless, the reaction over the prolonged period of time had a fast and a slower phase. Most likely, the slower phase was a result of product inhibition. Even though the products of hydrolysis, i.e., glucose and PNP, could not compete with **1β** in their binding with MINP(**3a**) (Table 1), as the substrate was consumed and more and more products formed, some level of product inhibition was expected at higher conversion, especially from the stronger binding *p*-nitrophenol.

Table 3 summarizes the Michaelis–Menten parameters of MINP(**3a**)+**2a** determined at different pHs (entries 1–5). Both k_{cat} and the catalytic efficiency (k_{cat}/K_m) showed a maximum at pH 6, similar to that in Figure 1b. The pH effect should reflect at least three factors—the binding of the substrate, the binding of the acid cofactor, and the fraction of the acid cofactor in the protonated form near the bound substrate. The K_m values of **1β** in Table 3 (entries 1–5) showed a monotonous decrease at increasing pH, indicating the binding of substrate became weaker in less acidic solutions. This was also the trend observed in the ITC-determined binding constants for the substrate (Table 1). On the other hand, ITC showed that the binding of the acid cofactor increased at lower pH, and a low pH should help the cofactor stay protonated. Thus, the maximum at pH 6 for the catalytic hydrolysis should come from the opposing pH effects of the substrate-binding and the acid-cofactor-binding.

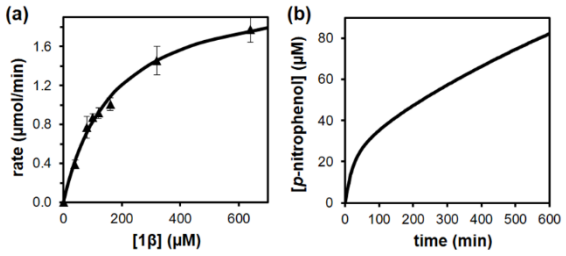

Figure 2. (a) Michaelis-Menten plot for the hydrolysis of **1β** by MINP(**3a**)+**2a** in a 10 mM MES buffer (pH 6) at 40 °C. [MINP(**3a**)] = 5 μM. [**2a**] = 10 μM. (b) Amount of PNP formed as a function of time, calculated from an extinction coefficient of ε_{320} = 0.0084 $\mu M^{-1}cm^{-1}$.

Selectivity of MINP-based glycosidase. As mentioned earlier in the paper, substrate selectivity is the most difficult challenge in the hydrolysis of glycans. Figure 3a shows the hydrolysis of a range of *p*-nitrophenyl D-glycopyranosides in pH 6 buffer at 40 °C. Under our standard catalyst loading (5 mol % MINP(**3a**) and 10 mol % **2a**), **1β** hydrolyzed faster than **1α** by 11.4 times (Figure 3b). According to the ITC measurements, MINP(**3a**) bound **1β** more strongly than **1α**,by 3.4 times (Table1, entries 1 & 4). Since binding was a single event and catalysis required many turnovers, it was reasonable that the MINP catalyst was more sensitive to structural changes in catalysis than in binding.[55] The selectivity was also observed when an equimolar mixture of **1α** and **1β** was used (Figures S58–63).

Among the three β anomers, the order of reactivity observed was glucoside (**1β**) > mannoside (**9β**) > galactoside (**10β**), as shown by

Table 3. Michaelis–Menten Parameters for MINP(**3a**)+**2a** in the hydrolysis of *p*-nitrophenyl glycopyransides.[a]

entry	substrate	pH	V_{max} (μM/min)	K_m (μM)	k_{cat} ($\times 10^{-3}$ s^{-1})	k_{cat}/K_m (M^{-1} min^{-1})
1	**1β**	5.5	1.26 ± 0.08	361 ± 46	4.20 ± 0.26	698
2	**1β**	6.0	2.23 ± 0.08	169 ± 15	7.44 ± 0.26	2640
3	**1β**	6.5	0.88 ± 0.03	147 ± 14	2.94 ± 0.10	1198
4	**1β**	7.0	0.07 ± 0.01	117 ± 17	0.23 ± 0.01	118
5	**1β**	7.4	0.06 ± 0.01	114 ± 15	0.18 ± 0.01	96
6	**1α**	6.0	1.11 ± 0.04	311 ± 23	3.70 ± 0.14	714
7	**9β**	6.0	1.57 ± 0.02	183 ± 9	5.24 ± 0.06	1716
8	**9α**	6.0	1.05 ± 0.04	726 ± 50	3.50 ± 0.14	290
9	**10β**	6.0	1.14 ± 0.04	223 ± 21	3.80 ± 0.14	1022
10	**10α**	6.0	0.73 ± 0.04	508 ± 55	2.44 ± 0.14	288

[a] All reaction rates were measured in 10 mM buffer at 40 °C (Figures S43-S51). [substrate] = 100 μM. [**2a**] = 10 μM. and [MINP] = 5 μM.

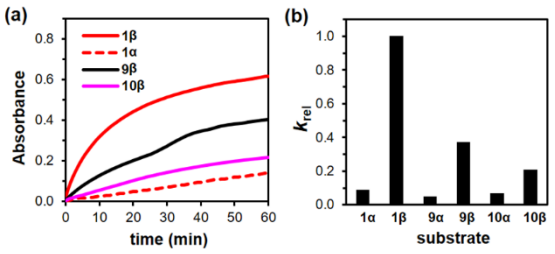

Figure 3. (a) Absorbance at 320 as a function of time for the hydrolysis of **1β**, **1α**, **9β**, and **10β** catalyzed by MINP(**3a**)+**2a** in a 10 mM MES buffer (pH 6.0) at 40 °C. Hydrolyses of **9α** and **10α** are omitted for clarity. [substrate] = 100 μM. [MINP(**3a**)] = 5 μM. [**2a**] = 10 μM. (b) Rate constants for the hydrolysis of different substrates normalized to that of glucoside **1β** (for the rate constants, see Table S1).

Figure 3b. The trend was in line with the boronic acid-binding, as the mannoside had the same *trans*-4,6-diol involved in boronate formation as the targeted substrate (**1β**), whereas the galactoside had a *cis*-4,6-diol. Both the K_a values in Table 1 and the K_m values in Table 3 supported this view. Meanwhile, all three α anomers exhibited similar reactivities and were significantly less reactive than the β substrates. The low catalytic efficiencies (k_{cat}/K_m) for the α anomers resulted from a combination of weak binding and slower catalytic turnovers (Table 3).

Our ITC binding data showed that galactoside **10β** was bound less strongly than glucoside **1α** (Table 1). Yet, their reactivity was just the opposite. This seemingly unusual behavior is actually consistent with the earlier postulation that MINP(**3a**) might have accommodated the PNP group of **1α** by its exceedingly large hydrophobic pocket when its matched glycan entered the sugar-binding site. In the presence of acid cofactor **2a**, however, such benefit would no longer be available to **1α** because the PNP pocket was designed for the β anomer. The explanation was supported by the K_m values in Table 3 that showed the binding in catalysis followed the order of **1β** > **9β** > **10β** > **1α**. Under such a scenario, **1α** would most likely adopt similar configuration as the doubly mismatched **9α** and **10α**, with the PNP group in the active site and the glycan outside. All three α-glycosides indeed exhibited similar, low activity in Figure 3.

Controlled, tunable selectivity for glycan hydrolysis has not been achieved by synthetic catalysts. To demonstrate the generality of our method, we synthesized template **3c** from commercially available O-(2,4-dinitrophenyl)-hydroxylamine **11** (Scheme 2). Reductive amination of dodecanal using this compound yielded the alkylated **12**, which reacted with D-mannose under acidic conditions yielded the thermodynamically favored α-mannoside **13**.[56]

Template–FM complex **3c** had a number features that differed from **3a**,**b**. First, instead of an isolable compound, **3c** was formed in situ from vinylphenylboroxole **14** under our imprinting conditions. Boroxole is known to be a stronger binding group for sugars.[25] Our previous study showed that boronate product could survive the micellar imprinting process, apparently with the amphiphilic, anionic boronate stabilized by the cationic micelle.[57] Second, the hydrophobic group in **3c** was a dodecyl, much smaller than the adamantyl in **3a**,**b**. The binding for the acid cofactor (i.e., lauric acid) was expected to be lower. Third, there are some significant mismatches between

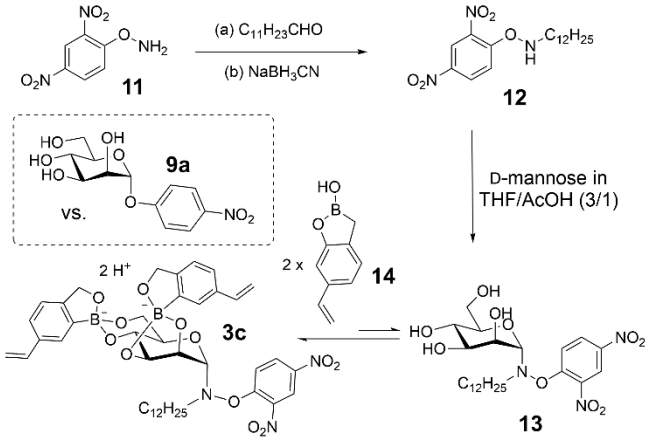

Scheme 2. In situ formation of template–FM complex **3c** and synthesis of **13**.

the template **13** and the targeted mannoside **9α**. The *ortho*-nitro group on **13** was added mainly because the corresponding starting material (**11**) was commercially available. In addition, two atoms (N and O) were in between the anomeric carbon and the phenyl group in **13** and only one in **9α**. At the outset of the project, it was unclear to us whether such discrepancy could be tolerated by the catalysis but the facile synthesis of **13** using commercially available starting materials and unprotected sugar was worth the risk in our mind.

To our delight, MINP(**3c**) showed significant binding to the targeted mannoside **9α** (Table 4). The binding increased with a higher FM/template ratio (entries 1–3) and the binding constant at the higher FM/template ratio was even higher than that of **1β** by MINP(**3a**). It seems any discrepancy between the imprinted site and **9α** was compensated by the double boronates formed by a mannoside, from the 2,3-*cis*-diol and 4,6-*trans*-diol. The binding also showed significant selectivity. Among the different glycoside analogues, **9β** and **1α** had a similar binding constant, about 6–7 times lower than that for **9α**. The difference corresponded to a difference of >1 kcal/mol in binding free energy and was caused by the inversion of a single stereogenic center (at C1 or C2). Inversion of two or more stereogenic centers (for **1β**, **10α**, and **10β**) weakened the binding even more. Lauric acid was found to give a binding constant of $K_a = 22.7 \times 10^4\ M^{-1}$ (Table 4, entry 9). Although the binding was weaker than that for 1-adamantanecarboxylic acid by MINP(**3a**), it was still substantial.

Importantly, MINP(**3c**) showed strong selectivity for the targeted **9α** as well (Figure 4a). When all the α anomers are compared, the most reactive one clearly was **9α**, followed by **1α**, and then **10α** (Figure 4b). The order was the same observed in the ITC binding (Table 3). For the glycosides derive from the same sugar, the α anomer always hydrolyzed faster than the β anomer. The trend was completely opposite to that observed in Figure 3b for MINP(**3a**), underscoring the predictability of the selectivity and, also, the reliability of the imprinting process. Among the different glycans, the highest selectivity was achieved for the mannosides (α/β = 7.2:1), consistent with successful imprinting. Table 5 summarizes the Michaelis–Menten parameters of MINP(**3c**). Once again, the higher catalytic efficiency for the targeted α mannoside over other analogues was a result of stronger substrate binding and faster catalytic turnover.

Table 4. ITC binding data for *p*-nitrophenyl glycopyranosides and acid catalysts by MINP(**3c**).[a]

entry	MINP	[**14**]/[**13**]	guest	K_a ($\times 10^4$ M^{-1})	ΔG (kcal/mol)	ΔH (kcal/mol)	$T\Delta S$ (kcal/mol)	N [b]
1	MINP(**3c**)	1	9α	8.49 ± 0.54	-6.72	-3.79 ± 0.08	2.93	0.94 ± 0.01
2	MINP(**3c**)	2	9α	12.50 ± 0.46	-6.95	-3.14 ± 0.03	3.81	1.02 ± 0.01
3	MINP(**3c**)	3	9α	16.30 ± 0.32	-7.11	-3.84 ± 0.01	3.27	0.94 ± 0.01
4	MINP(**3c**)	2	9β	1.78 ± 0.10	-5.79	-3.97 ± 0.18	1.82	0.99 ± 0.04
5	MINP(**3c**)	2	1α	1.94 ± 0.23	-5.85	-1.46 ± 0.07	4.39	1.06 ± 0.04
6	MINP(**3c**)	2	1β	0.91 ± 0.08	-5.40	-2.55 ± 0.14	2.85	1.50 ± 0.06
7	MINP(**3c**)	2	10α	0.88 ± 0.06	-5.38	-2.11 ± 0.09	3.27	1.31 ± 0.04
8	MINP(**3c**)	2	10β	0.81 ± 0.06	-5.33	-1.01 ± 0.04	4.32	1.46 ± 0.04
9	MINP(**3c**)	2	lauric acid[c]	22.7 ± 1.5	-7.30	-3.06 ± 0.02	4.24	1.07 ± 0.01

[a] The FM 4-vinylbenzoboroxole/template ratio in the MINP synthesis was 1:2 unless otherwise indicated. The titrations were performed in 10 mM MES buffer at pH 6.0. The ITC titration curves were reported in the Supporting Information (Figures S28-S36). [b] N is the average number of binding site per nanoparticle measured by ITC curve fitting. [b] Titrations were performed in 10 mM MES buffer (pH 6.0) with 2% (v/v) DMSO.

Table 5. Michaelis–Menten Parameters for the MINP(**3c**) with lauric acid in the hydrolysis of PNP-glycopyranoside.[a]

entry	substrate	V_{max} (μM/min)	K_m (μM)	k_{cat} ($\times 10^{-3}$ s^{-1})	k_{cat}/K_m (M^{-1} min^{-1})
1	**1β**	0.30 ± 0.01	129 ± 7	1.00 ± 0.04	464
2	**1α**	0.58 ± 0.02	65 ± 8	1.94 ± 0.06	1776
3	**9β**	0.47 ± 0.01	105 ± 9	1.56 ± 0.04	896
4	**9α**	0.72 ± 0.01	25 ± 2	2.40 ± 0.04	5692
5	**10β**	0.21 ± 0.01	448 ± 59	0.70 ± 0.04	94
6	**10α**	0.23 ± 0.01	284 ± 35	0.76 ± 0.04	162

[a] All reaction rates were measured in 10 mM buffer at pH 6.0 at 40 °C (Figures S52-S57). [substrate] = 100 μM. [lauric acid] = 10 μM. [MINP(**3c**)] = 5 μM.

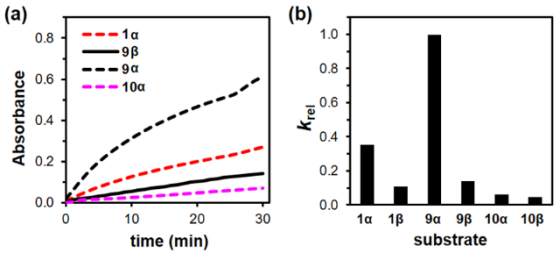

Figure 4. (a) Absorbance at 320 as a function of time for the hydrolysis of **1α**, **9β**, **9α**, and **10α** catalyzed by MINP(**3c**) and lauric acid in a 10 mM MES buffer (pH 6.0) at 40 °C. Hydrolyses of **1β** and **10β** are omitted for clarity. [Substrate] = 100 μM. [MINP] = 5 μM. [lauric acid] = 10 μM. (b) Rate constants and relative constant for the hydrolysis of different substrates normalized to that of mannoside **9α** (for the rate constants, see Table S2).

CONCLUSIONS

This work demonstrates that selective hydrolysis of aryl glycosides can be achieved in a straightforward, rational manner using molecularly imprinted cross-linked micelles. A significant feature of the imprinting-based method is facile construction of complex-shaped catalytic active sites. In enzymes, such sites are formed by the folding and aggregation of long peptides. In small-molecule-based artificial enzymes, a tremendous effort goes into the synthesis of cavity-containing host structures.[36-38] Thanks to the 1-pot, 2-day preparation of MINP (after the cross- linkable surfactant, surface-cross-linker, surface ligand, and the template–FM complex became available), construction of such sites are simplified largely into standard syntheses of small-molecule templates, followed by covalent capture and templated polymerization. In enzymatic catalysis, it is frequently observed that "relatively small difference in substrate structure that do not affect the chemical reactivity of the substrate have large effects on k_{cat}".[58] Although our synthetic glycosidase was quite primitive in design and improvements are clearly needed, it was good that such a trend was already observed.

Another interesting discovery, which was counterintuitive, was that the weaker carboxylic acid in our synthetic glycosidase turned out as a more active catalyst than the stronger sulfonic acid. Equally important was that small discrepancies between the template and the targeted substrate were well tolerated—a flexibility very useful in the construction of imprinted synthetic enzymes in general.

ASSOCIATED CONTENT

Supporting Information

Experimental details, ITC titration curves, Michaelis-Menten data, and additional figures. This material is available free of charge via the Internet at http://pubs.acs.org.

AUTHOR INFORMATION

Corresponding Author

*zhaoy@iastate.edu

Notes

Iowa State University Research Foundation has filed a patent application on the technology.

ACKNOWLEDGMENT

We thank NSF (CHE-1708526) and NIGMS (R01GM138427) for supporting the research.

REFERENCES

(1) Bertozzi, C. R.; Kiessling, L. L. Chemical Glycobiology. *Science* **2001**, *291*, 2357-2364.
(2) Kamerling, J. P.; Boons, G.-J.: *Comprehensive Glycoscience: From Chemistry to Systems Biology*; 1st ed.; Elsevier: Amsterdam ; Boston, 2007.
(3) Palaniappan, K. K.; Bertozzi, C. R. Chemical Glycoproteomics. *Chem. Rev.* **2016**, *116*, 14277-14306.
(4) (U.S.)., N. R. C.: *Transforming Glycoscience : A Roadmap for the Future*; National Academies Press: Washington, D.C., 2012.
(5) Davies, G. J.; Gloster, T. M.; Henrissat, B. Recent Structural Insights into the Expanding World of Carbohydrate-Active Enzymes. *Curr. Opin. Struct. Biol.* **2005**, *15*, 637-645.
(6) Wahlström, R. M.; Suurnäkki, A. Enzymatic Hydrolysis of Lignocellulosic Polysaccharides in the Presence of Ionic Liquids. *Green Chem.* **2015**, *17*, 694-714.
(7) Davis, A. P.; James, T. D.: *Carbohydrate Receptors*; Wiley-VCH: Weinheim, 2005.
(8) Rousseau, C.; Nielsen, N.; Bols, M. An Artificial Enzyme That Catalyzes Hydrolysis of Aryl Glycosides. *Tetrahedron Lett* **2004**, *45*, 8709-8711.
(9) Ortega-Caballero, F.; Rousseau, C.; Christensen, B.; Petersen, T. E.; Bols, M. Remarkable Supramolecular Catalysis of Glycoside Hydrolysis by a Cyclodextrin Cyanohydrin. *J. Am. Chem. Soc.* **2005**, *127*, 3238-3239.
(10) Striegler, S.; Barnett, J. D.; Dunaway, N. A. Glycoside Hydrolysis with Sugar-Templated Microgel Catalysts. *ACS Catal.* **2012**, *2*, 50-55.
(11) Sharma, B.; Striegler, S. Crosslinked Microgels as Platform for Hydrolytic Catalysts. *Biomacromolecules* **2018**, *19*, 1164-1174.
(12) Samanta, M.; Krishna, V. S. R.; Bandyopadhyay, S. A Photoresponsive Glycosidase Mimic. *Chem. Commun.* **2014**, *50*, 10577-10579.
(13) Yu, Z.; Cowan, J. A. Design of Artificial Glycosidases: Metallopeptides That Remove H Antigen from Human Erythrocytes. *Angew. Chem. Int. Ed.* **2017**, *56*, 2763-2766.
(14) Duan, L.; Zangiabadi, M.; Zhao, Y. Synthetic Lectins for Selective Binding of Glycoproteins in Water. *Chem. Commun.* **2020**, *56*, 10199-10202.
(15) Zangiabadi, M.; Zhao, Y. Selective Binding of Complex Glycans and Glycoproteins in Water by Molecularly Imprinted Nanoparticles. *Nano Lett.* **2020**, *20*, 5106-5110.
(16) Wulff, G.; Vesper, W. Enzyme-Analogue Built Polymers .8. Preparation of Chromatographic Sorbents with Chiral Cavities for Racemic-Resolution. *J. Chromatogr.* **1978**, *167*, 171-186.
(17) Wulff, G.; Schauhoff, S. Enzyme-Analog-Built Polymers. 27. Racemic Resolution of Free Sugars with Macroporous Polymers Prepared by Molecular Imprinting. Selectivity Dependence on the Arrangement of Functional Groups Versus Spatial Requirements. *J. Org. Chem.* **1991**, *56*, 395-400.
(18) Wulff, G. Molecular Imprinting in Cross-Linked Materials with the Aid of Molecular Templates— a Way Towards Artificial Antibodies. *Angew. Chem. Int. Ed. Engl.* **1995**, *34*, 1812-1832.
(19) James, T. D.; Phillips, M. D.; Shinkai, S.: *Boronic Acids in Saccharide Recognition*; RSC Publishing: Cambridge, 2006.
(20) Kim, K. T.; Cornelissen, J. J. L. M.; Nolte, R. J. M.; van Hest, J. C. M. Polymeric Monosaccharide Receptors Responsive at Neutral pH. *J. Am. Chem. Soc.* **2009**, *131*, 13908-13909.
(21) Pal, A.; Bérubé, M.; Hall, D. G. Design, Synthesis, and Screening of a Library of Peptidyl Bis(Boroxoles) as Oligosaccharide Receptors in Water: Identification of a Receptor for the Tumor Marker Tf-Antigen Disaccharide. *Angew. Chem. Int. Ed.* **2010**, *49*, 1492-1495.
(22) Wu, X.; Li, Z.; Chen, X.-X.; Fossey, J. S.; James, T. D.; Jiang, Y.-B. Selective Sensing of Saccharides Using Simple Boronic Acids and Their Aggregates. *Chem. Soc. Rev.* **2013**, *42*, 8032-8048.
(23) Bull, S. D.; Davidson, M. G.; Van den Elsen, J. M. H.; Fossey, J. S.; Jenkins, A. T. A.; Jiang, Y. B.; Kubo, Y.; Marken, F.; Sakurai, K.; Zhao, J. Z.; James, T. D. Exploiting the Reversible Covalent Bonding of Boronic Acids: Recognition, Sensing, and Assembly. *Acc. Chem. Res.* **2013**, *46*, 312-326.
(24) Kim, H.; Kang, Y. J.; Kang, S.; Kim, K. T. Monosaccharide-Responsive Release of Insulin from Polymersomes of Polyboroxole Block Copolymers at Neutral Ph. *J. Am. Chem. Soc.* **2012**, *134*, 4030-4033.
(25) Dowlut, M.; Hall, D. G. An Improved Class of Sugar-Binding Boronic Acids, Soluble and Capable of Complexing Glycosides in Neutral Water. *J. Am. Chem. Soc.* **2006**, *128*, 4226-4227.
(26) Bérubé, M.; Dowlut, M.; Hall, D. G. Benzoboroxoles as Efficient Glycopyranoside-Binding Agents in Physiological Conditions: Structure and Selectivity of Complex Formation. *J. Org. Chem.* **2008**, *73*, 6471-6479.
(27) Wulff, G. Enzyme-Like Catalysis by Molecularly Imprinted Polymers. *Chem. Rev.* **2002**, *102*, 1-28.
(28) Wulff, G.; Liu, J. Design of Biomimetic Catalysts by Molecular Imprinting in Synthetic Polymers: The Role of Transition State Stabilization. *Acc. Chem. Res.* **2012**, *45*, 239-247.
(29) Emgenbroich, M.; Wulff, G. A New Enzyme Model for Enantioselective Esterases Based on Molecularly Imprinted Polymers. *Chem.-Eur. J.* **2003**, *9*, 4106-4117.
(30) Liu, J.-q.; Wulff, G. Functional Mimicry of Carboxypeptidase a by a Combination of Transition State Stabilization and a Defined Orientation of Catalytic Moieties in Molecularly Imprinted Polymers. *J. Am. Chem. Soc.* **2008**, *130*, 8044-8054.
(31) Kirsch, N.; Hedin-Dahlström, J.; Henschel, H.; Whitcombe, M. J.; Wikman, S.; Nicholls, I. A. Molecularly Imprinted Polymer Catalysis of a Diels-Alder Reaction. *J. Mol. Catal. B: Enzym.* **2009**, *58*, 110-117.
(32) Chen, Z. Y.; Xu, L.; Liang, Y.; Zhao, M. P. pH-Sensitive Water-Soluble Nanospheric Imprinted Hydrogels Prepared as Horseradish Peroxidase Mimetic Enzymes. *Adv. Mater.* **2010**, *22*, 1488-1492.
(33) Servant, A.; Haupt, K.; Resmini, M. Tuning Molecular Recognition in Water-Soluble Nanogels with Enzyme-Like Activity for the Kemp Elimination. *Chem.-Eur. J.* **2011**, *17*, 11052-11059.
(34) Shen, X.; Huang, C.; Shinde, S.; Jagadeesan, K. K.; Ekström, S.; Fritz, E.; Sellergren, B. Catalytic Formation of Disulfide Bonds in Peptides by Molecularly Imprinted Microgels at Oil/Water Interfaces. *ACS Appl. Mater. Interfaces* **2016**, *8*, 30484-30491.
(35) Zheng, A.-X.; Gong, C.-B.; Zhang, W.-J.; Tang, Q.; Huang, H.-R.; Chow, C.-F.; Tang, Q. An Amphiphilic and Photoswitchable Organocatalyst for the Aldol Reaction Based on a Product-Imprinted Polymer. *Mol. Catal.* **2017**, *442*, 115-125.
(36) Breslow, R.: *Artificial Enzymes*; Wiley-VCH: Weinheim, 2005.
(37) Kirby, A. J.; Hollfelder, F.: *From Enzyme Models to Model Enzymes*; Royal Society of Chemistry: Cambridge, UK, 2009.
(38) Raynal, M.; Ballester, P.; Vidal-Ferran, A.; van Leeuwen, P. W. N. M. Supramolecular Catalysis. Part 2: Artificial Enzyme Mimics. *Chem. Soc. Rev.* **2014**, *43*, 1734-1787.
(39) Awino, J. K.; Gunasekara, R. W.; Zhao, Y. Selective Recognition of D-Aldohexoses in Water by Boronic Acid-Functionalized, Molecularly Imprinted Cross-Linked Micelles. *J. Am. Chem. Soc.* **2016**, *138*, 9759-9762.
(40) Awino, J. K.; Zhao, Y. Protein-Mimetic, Molecularly Imprinted Nanoparticles for Selective Binding of Bile Salt Derivatives in Water. *J. Am. Chem. Soc.* **2013**, *135*, 12552-12555.
(41) Schmidtchen, F. P.: Isothermal Titration Calorimetry in Supramolecular Chemistry. In *Supramolecular Chemistry: From Molecules to Nanomaterials*; Steed, J. W., Gale, P. A., Eds.; Wiley: Weinheim, 2012.
(42) Wang, B.; Boons, G.-J.: *Carbohydrate Recognition: Biological Problems, Methods, and Applications*; Wiley: Hoboken, N.J., 2011.
(43) Yan, J.; Springsteen, G.; Deeter, S.; Wang, B. The Relationship among pK_a, pH, and Binding Constants in the Interactions between Boronic Acids and Diols—It Is Not as Simple as It Appears. *Tetrahedron* **2004**, *60*, 11205-11209.
(44) Tanford, C.: *The Hydrophobic Effect: Formation of Micelles and Biological Membranes*; 2nd ed.; Krieger: Malabar, Fla., 1991.
(45) Ben-Naim, A.: *Hydrophobic Interactions*; Plenum Press: New York, 1980.
(46) Southall, N. T.; Dill, K. A.; Haymet, A. D. J. A View of the Hydrophobic Effect. *J. Phys. Chem. B* **2002**, *106*, 521-533.
(47) Westheimer, F. H. Coincidences, Decarboxylation, and Electrostatic Effects. *Tetrahedron* **1995**, *51*, 3-20.
(48) Matulis, D.; Bloomfield, V. A. Thermodynamics of the Hydrophobic Effect. I. Coupling of Aggregation and Pka Shifts in Solutions of Aliphatic Amines. *Biophys. Chem.* **2001**, *93*, 37-51.

(49) Arifuzzaman, M. D.; Zhao, Y. Water-Soluble Molecularly Imprinted Nanoparticle Receptors with Hydrogen-Bond-Assisted Hydrophobic Binding. *J. Org. Chem.* **2016**, *81*, 7518-7526.
(50) Fa, S.; Zhao, Y. General Method for Peptide Recognition in Water through Bioinspired Complementarity. *Chem. Mater.* **2019**, *31*, 4889-4896.
(51) Duan, L.; Zhao, Y. Zwitterionic Molecularly Imprinted Cross-Linked Micelles for Alkaloid Recognition in Water. *J. Org. Chem.* **2019**, *84*, 13457-13464.
(52) Zangiabadi, M.; Zhao, Y. Molecularly Imprinted Polymeric Receptors with Interfacial Hydrogen Bonds for Peptide Recognition in Water. *ACS Appl. Polym. Mater.* **2020**, *2*, 3171-3180.
(53) Awino, J. K.; Gunasekara, R. W.; Zhao, Y. Sequence-Selective Binding of Oligopeptides in Water through Hydrophobic Coding. *J. Am. Chem. Soc.* **2017**, *139*, 2188-2191.
(54) Chen, K.; Zhao, Y. Effects of Nano-Confinement and Conformational Mobility on Molecular Imprinting of Cross-Linked Micelles. *Org. Biomol. Chem.* **2019**, *17*, 8611-8617.
(55) Arifuzzaman, M.; Zhao, Y. Artificial Zinc Enzymes with Fine-Tuned Catalytic Active Sites for Highly Selective Hydrolysis of Activated Esters. *ACS Catal* **2018**, *8*, 8154-8161.
(56) Peri, F.; Dumy, P.; Mutter, M. Chemo- and Stereoselective Glycosylation of Hydroxylamino Derivatives: A Versatile Approach to Glycoconjugates. *Tetrahedron* **1998**, *54*, 12269-12278.
(57) Gunasekara, R. W.; Zhao, Y. A General Method for Selective Recognition of Monosaccharides and Oligosaccharides in Water. *J. Am. Chem. Soc.* **2017**, *139*, 829-835.
(58) Jencks, W. P. Binding-Energy, Specificity, and Enzymic Catalysis - Circe Effect. *Adv. Enzymol. Relat. Areas Mol. Biol.* **1975**, *43*, 219-410.

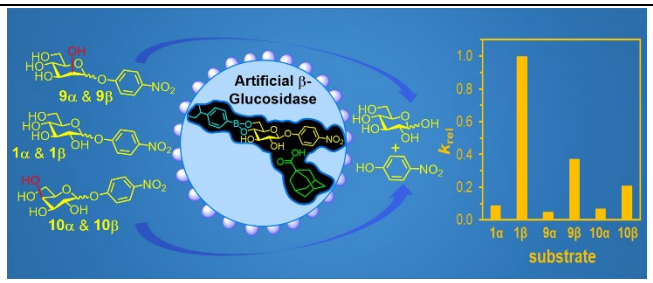
9α & 9β
1α & 1β
10α & 10β
Artificial β-Glucosidase
1.0
0.8
0.6
0.4
0.2
0.0
k_{rel}
1α 1β 9α 9β 10α 10β
substrate